Dark matter-motivated searches for exotic fourth-generation mirror quarks in Tevatron and early LHC data

Johan Alwall,[1] Jonathan L. Feng,[2] Jason Kumar,[3] and Shufang Su[4]

[1]*Department of Physics and National Center for Theoretical Sciences, National Taiwan University, Taipei 10617, Taiwan*
[2]*Department of Physics and Astronomy, University of California, Irvine, California 92697, USA*
[3]*Department of Physics and Astronomy, University of Hawai'i, Honolulu, Hawaii 96822, USA*
[4]*Department of Physics, University of Arizona, Tucson, Arizona 85721, USA*
(Received 2 March 2010; published 17 June 2010)

We determine the prospects for finding dark matter at the Tevatron and LHC through the production of exotic fourth-generation mirror quarks T' that decay through $T' \to tX$, where X is dark matter. The resulting signal of $t\bar{t} + \not{E}_T$ has not previously been considered in searches for fourth-generation quarks, but there are both general and specific dark matter motivations for this signal, and with slight modifications, this analysis applies to any scenario where invisible particles are produced in association with top quarks. Current direct and indirect bounds on such exotic quarks restrict their masses to be between 300 and 600 GeV, and the dark matter's mass may be anywhere below $m_{T'}$. We simulate the signal and main backgrounds with MADGRAPH/MADEVENT-PYTHIA-PGS4. For the Tevatron, we find that an integrated luminosity of 20 fb^{-1} will allow 3σ discovery up to $m_{T'} = 400$ GeV and 95% exclusion up to $m_{T'} = 455$ GeV. For the 10 TeV LHC with 300 pb^{-1}, the discovery and exclusion sensitivities rise to 490 GeV and 600 GeV. These scenarios are therefore among the most promising for dark matter at colliders. Perhaps most interestingly, we find that dark matter models that can explain results from the DAMA, CDMS, and CoGeNT collaborations can be tested with high statistical significance using data already collected at the Tevatron and have extraordinarily promising implications for early runs of the LHC.

I. INTRODUCTION

One of the great hopes for current and future particle colliders is that they will be able to produce dark matter. In this study, we determine the prospects for finding dark matter through the production of exotic fourth-generation mirror quarks T' that decay through $T' \to tX$, where X is dark matter. These are fourth-generation mirror quarks because they are chiral under standard model gauge groups, but the left- and right-handed fermions have the opposite charge to those carried by the quarks of the first three generations. These new quarks are exotic because they also carry charge under an unbroken hidden sector symmetry which stabilizes the dark matter candidate, thus necessitating a hidden sector decay channel to the dark matter. We will refer to them as "new exotic quarks" from now on. Current direct and indirect bounds on such exotic quarks restrict their mass range to 300 GeV $\lesssim m_{T'} \lesssim$ 600 GeV. Our analysis is valid for all dark matter masses up to $m_{T'} - m_W - m_b$, although there are special reasons to be interested in very light X particles, with $m_X \sim$ 1–10 GeV.

There are both general and specific dark matter motivations for this signal. Starting with the general motivation, one of the few things that is absolutely certain about dark matter is that it must be long-lived on cosmological time scales. This is typically achieved by giving dark matter a charge under an unbroken discrete or continuous symme-

try, which makes it absolutely stable. None of the unbroken symmetries of the standard model (SM) will do for this purpose, so the dark matter particle must be charged under a new unbroken symmetry.

There are then two options. The dark matter, with its stabilizing "dark charge," may have only gravitational interactions with the SM. In this case, dark matter may have interesting astrophysical signals [1,2], but it cannot be discovered at colliders.

Alternatively, the dark matter may be coupled to SM particles f through connector particles Y that have both dark and SM charges to make XYf couplings possible. X may or may not have SM weak interactions. However, Y necessarily has SM charge. It can therefore be produced at colliders, and so dark matter can be discovered through Y production followed by $Y \to fX$. Since the energy frontier is dominated by hadron colliders for the foreseeable future, the most promising case is where Y is strongly interacting. Supersymmetric (universal extra dimension) models provide a concrete example of this, where the dark matter is neutralinos [3,4] (Kaluza-Klein (KK) gauge bosons [5,6]), the connector particles are squarks (KK quarks), and the stabilizing symmetry is R-parity (KK-parity). Here we consider the case where the dark matter has no SM gauge interactions, the connector particles are exotic quarks, and the stabilizing symmetry may be either discrete or continuous [7,8]. Note, however, that with minor modifications, our analysis applies much more generally, both to the

supersymmetric and extra dimensional scenarios just mentioned, as well as to many other dark matter scenarios motivated by the general chain of reasoning given above.

These scenarios also have a more speculative, but at the same time more specific and tantalizing, dark matter motivation. The DAMA experiment sees an 8.9σ signal in the annual modulation of scattering rates that can potentially be explained by dark matter [9,10]. Uncertainties from both astrophysics [11] and detector response [12] open the possibility that DAMA can be explained without conflicting with other experiments by a light dark matter particle with mass $m_X \sim 1$–10 GeV elastically scattering off nucleons with spin-independent (SI) cross section $\sigma_{SI} \sim 10^{-2}$–10^{-5} pb [13]. This explanation is supported by unexplained events recently reported by the CoGeNT Collaboration [14], which, if interpreted as a dark matter signal, are best fit by dark matter with $m_X \sim 9$ GeV and $\sigma_{SI} \sim 6.7 \times 10^{-5}$ pb. The low mass and high cross sections preferred by DAMA and CoGeNT are consistent with the recent bounds and results from CDMS [15].

Such large cross sections are several orders of magnitude larger than those of typical weakly interacting massive particles (WIMPs). As we review below, however, they are easily obtained if the dark matter particle scatters through $Xq \to Q' \to Xq$, where Q' is a new exotic quark. Furthermore, this scenario naturally emerges in WIMPless dark matter models, where dark matter not only can have the correct m_X and σ_{SI} for DAMA and CoGeNT, but also naturally has the correct thermal relic density [7,8]. This scenario is a special case of the general framework described above and, as discussed in Sec. II, particularly motivates the case where dark matter couples to third-generation quarks and the X particles are light.

Given all of these motivations, we explore here the detection prospects for new exotic quarks decaying directly to dark matter. This signal differs from most supersymmetry searches, which typically assume that decays to dark matter are dominated by cascade decays. The new exotic quarks examined here also differ from the fourth-generation quarks that are typically studied, because they are charged under a new symmetry under which SM particles are neutral. This forbids decays to SM quarks, such as $T' \to Wb$ and $B' \to Wt$, which are the basis for most standard fourth-generation quark searches. Instead, all Q' decays must necessarily produce hidden sector particles charged under the new symmetry, with the lightest such particle being X, the dark matter. This leads to the signal of $t\bar{t} + \not{E}_T$, which has previously not been considered in searches for fourth-generation quarks. In addition, as emphasized earlier, this type of signal appears in a general set of dark matter motivated models, as well as other new physics scenarios, such as little Higgs models with T-parity conservation [16] and models in which baryon and lepton number are gauge symmetries [17]. The results of our analyses can be easily applied to these other models.

We will find that T' pair production followed by $T' \to tX$ leads to $\not{E}_T$ signals that may be discovered at the Tevatron with 10 fb^{-1} of integrated luminosity, or at the LHC with integrated luminosities of as little as $\sim$100 pb^{-1}.

In Sec. II we detail the dark matter motivations and define the model we explore. In Sec. III we summarize the current theoretical and experimental constraints on new exotic quarks. We then describe the details of our signal and background simulations and cut analysis in Sec. IV. In Sec. V we present the prospects for discovering or excluding these new exotic fourth-generation quark scenarios with Tevatron and early LHC data. We conclude with a discussion of future prospects in Sec. VI.

II. DARK MATTER MODELS WITH EXOTIC QUARKS

A. WIMPless dark matter

As discussed above, in this work we consider the case where dark matter has a charge under some new symmetry, but no SM gauge interactions. This dark matter is therefore not a typical WIMP, but it may nevertheless naturally appear in theories motivated by the gauge hierarchy problem and have the correct thermal relic density. This is the case for WIMPless dark matter models [7], supersymmetric models where the effects of a supersymmetry-breaking (SUSY-breaking) sector are transmitted to both the minimal supersymmetric SM (MSSM) sector and a hidden sector through gauge-mediation. The hidden sector superpartner mass scale is

$$m_{\text{hidden}} \propto g_{\text{hidden}}^2 \frac{F}{M_{\text{mess}}}, \tag{1}$$

where g_{hidden} is the hidden sector gauge coupling, F is the supersymmetry-breaking scale squared, and M_{mess} is the mass scale of the messenger particles. Because the MSSM superpartner masses are also generated by gauge-mediation from the same SUSY-breaking sector, we find

$$\frac{g_{\text{hidden}}^2}{m_{\text{hidden}}} \sim \frac{g_{\text{weak}}^2}{m_{\text{weak}}} \sim \frac{M_{\text{mess}}}{F}. \tag{2}$$

The ratio g^4/m^2 sets the annihilation cross section of a particle through gauge interactions, which in turn determines the thermal relic density of a stable particle [18]. The "WIMP miracle" is the remarkable coincidence that, for a stable WIMP with mass $m \sim m_{\text{weak}}$ and coupling $g \sim g_{\text{weak}}$, this thermal relic density is roughly that required by astrophysical observations. Equation (2) shows that our hidden sector candidate automatically has approximately the same annihilation cross section, and thus the same relic density.

If there are connectors Y with both dark and SM charge, WIMPless dark matter may have observable interactions through couplings XYf, where f are SM particles. In this case, WIMPless dark matter has many of the virtues and

implications commonly associated with WIMPs. In contrast to WIMPs, however, the WIMPless dark matter's mass need not be at the electroweak symmetry-breaking scale. It may be treated as a free parameter, which in turn determines the gauge coupling strength of the hidden sector. This freedom opens new possibilities for dark matter model parameters and new experimental search windows.

B. Explaining DAMA

The DAMA dark matter signal of annual modulation in direct detection has motivated a variety of explanations [19]. The canonical possibility, where WIMP dark matter with mass ~100 GeV elastically scatters, is excluded, as the required scattering cross section is in conflict with other experiments. Inelastic scattering [20–22], in which dark matter is assumed to scatter to another state that is ~100 keV heavier, has also been explored. Such scattering alleviates the conflict between different direct detection experiments, but is tightly constrained by neutrino bounds on dark matter annihilation in the Sun [23,24].

An alternative explanation is elastic scattering of a light dark matter particle with $m \sim 1$–10 GeV and large spin-independent nucleon scattering cross section $\sigma_{\rm SI} \sim 10^{-2}$–$10^{-5}$ pb [13], a region also supported by recent results from CoGeNT [14]. Such explanations are possible if the DAMA signal is enhanced by populations of dark matter in tidal streams [11] or detection thresholds are lowered by channeling [12], and may also require an unusual background spectrum for consistency [25]. In typical WIMP models, the required small masses and large cross sections are possible [26], but not at all generic.

In contrast, WIMPless dark matter provides a natural setting for the low mass explanation. In the example presented in Refs. [7,8], the dark matter particle in the hidden sector couples to the SM through Yukawa couplings

$$V = \lambda[X\bar{Q}'_L q_L + X\bar{B}'_R b_R + X\bar{T}'_R t_R]. \quad (3)$$

Each term may have a different coupling, but we assume equal couplings for simplicity. In Eq. (3), X is the dark matter, a complex scalar[1] charged under a discrete symmetry (hidden parity); $q_L^T \equiv (t_L, b_L)$, t_R, and b_R are the third-generation quarks of the SM; and $Q_L'^T \equiv (T'_L, B'_L)$, T'_R, and B'_R are the connectors, new exotic quarks. The Q' have hidden parity and are in the SM SU(3) × SU(2) × U(1)$_Y$ representations

$$Q'_L: \left(3, 2, \frac{1}{6}\right) \quad T'_R: \left(3, 1, \frac{2}{3}\right) \quad B'_R: \left(3, 1, -\frac{1}{3}\right). \quad (4)$$

The subscripts L and R refer to SU(2) doublets and singlets, respectively, not chirality; the chirality of the Q'_L, T'_R, and B'_R fields is opposite to their SM counterparts, and they

are therefore mirror quarks. Finally, the Q' receive mass through electroweak symmetry-breaking. One would typically need to add an entire fourth generation, including leptons, to cancel standard model hypercharge anomalies. Since exotic leptons do not couple to QCD, they are not as easily produced (or searched for) at hadron colliders, and we will not consider them further in this work.

The couplings of Eq. (3) imply scattering through $Xq \rightarrow Q' \rightarrow Xq$, where $q = b, t$. This induces a coupling to the gluons of the nucleon at one-loop [27]. As shown in Ref. [8], for $m_X \sim 1$–10 GeV, $m_{Q'} \sim 300$–500 GeV, and $\lambda \sim 0.3$–1, the coupling to b quarks produces a cross section $\sigma_{\rm SI}$ in the right range to explain DAMA and CoGeNT. For example, the best fit point for the CoGeNT data can be obtained with $m_X \sim 9$ GeV, $m_{Q'} \sim 400$ GeV, and $\lambda \sim 0.7$. The large cross section can be understood as follows: spin-independent scattering requires a chirality flip on the fermion line, which is typically suppressed by a small Yukawa coupling. But if the dark matter is a scalar, then a mass insertion on the Q' propagator provides the necessary chirality flip without suppressing $\sigma_{\rm SI}$, since the Q' are heavy and their Yukawa couplings are large. The explanation therefore requires that X is a scalar and the connectors are chiral fermions.

In fact, this mechanism is overly efficient. If the third-generation quarks are replaced by first-generation quarks in Eq. (3), the dark matter couples to nucleons at tree-level, and the desired $\sigma_{\rm SI}$ is achieved for couplings $\lambda \sim 0.03$ [7]. This is also perfectly acceptable and worth studying [28], but the required coupling for b quarks appears to be somewhat more natural and, in the general case where there are couplings to more than one generation, less constrained by flavor-changing neutral currents. In this study, we assume negligible couplings to first- and second-generation quarks and focus on the collider phenomenology of the case where the Q' decay directly to third-generation quarks.

If the dark matter is stabilized not by a discrete symmetry but by a continuous symmetry, Q'_L and T'_R/B'_R must have opposite dark charges to allow them to get a mass. The Yukawa couplings of Eq. (3) must therefore be generalized to

$$V' = \lambda[X_L\bar{Q}'_L q_L + X_R\bar{B}'_R b_R + X_R\bar{T}'_R t_R], \quad (5)$$

where X_L and X_R are two complex scalars with opposite dark charges. In general, X_L and X_R^* will mix to form mass eigenstates X_1 and X_2. The lighter state is the dark matter particle and can couple to both Q'_L and T'_R/B'_R. Despite slight additional complications, we therefore recover the discrete symmetry case, although there may now be additional decays $Q' \rightarrow qX_2$. For simplicity, we focus in the rest of this study on the discrete symmetry case with couplings given in Eq. (3).

---

[1]In a nonsupersymmetric context where the stabilizing symmetry is discrete, X could also be a real scalar.

III. EXISTING CONSTRAINTS

As with SM quarks, the new exotic quarks receive their mass through electroweak symmetry-breaking, and so $m_{Q'} = y_{Q'} v/\sqrt{2}$, where $v \simeq 246$ GeV. Perturbativity places an upper bound on $m_{Q'}$; requiring $\alpha_{Q'} \equiv y_{Q'}^2/4\pi \lesssim 1$ implies $m_{Q'} \lesssim 600$ GeV. The new exotic quark masses are also constrained by precision electroweak data. These constraints are not modified by the exotic and mirror features of the quarks we consider, and they imply $|m_{T'} - m_{B'}| \sim 50$ GeV, where some nondegeneracy is required [29]. New exotic quarks may also have many beneficial effects, for example, raising the Higgs boson mass in supersymmetric theories through their loop corrections, and enhancing Higgs boson production rates [29].

Direct searches place lower bounds on $m_{Q'}$. These searches are rather independent of the details of the couplings to the hidden sector. T' and B' production is dominated by QCD processes. In addition, the coupling λ only affects the T' and B' lifetimes. For all but extremely small λ, the T' and B' decay promptly.

With the model framework and assumptions given in Sec. II, the possible decays of the Q' are $T' \rightarrow tX$, $B' \rightarrow bX$, $T' \rightarrow W^{+(*)}B'$, and $B' \rightarrow W^{-(*)}T'$. If $|m_{T'} - m_{B'}| < m_W$, the decays $T' \rightarrow W^{+*}B'$ and $B' \rightarrow W^{-*}T'$ are strongly suppressed by kinematics. In the type of scenarios we are interested in here, the coupling between the Q' and X states is furthermore rather strong, which means that the decays $T' \rightarrow tX$ and $B' \rightarrow bX$ completely dominate. In our analysis below, we assume that $B(T' \rightarrow tX) = B(B' \rightarrow bX) = 1$.

B' pair production followed by $B' \rightarrow bX$ leads to a signature of $2b + \not{E}_T$, which is identical to the final state of bottom squark pair production followed by $\tilde{b} \rightarrow b\tilde{\chi}_1^0$. Searches for this supersymmetric signal have been carried at both CDF and D0 at the Tevatron. The D0 analysis, based on an integrated luminosity of 310 pb^{-1} from run II, implies $m_{\tilde{b}} > 222$ GeV (95% C.L.) for $m_{\tilde{\chi}_1^0} < 50$ GeV [30]; the corresponding CDF result using 295 pb^{-1} is $m_{\tilde{b}} > 193$ GeV (95% C.L.) [31]. Taking into account the difference in $B'\bar{B}'$ and $\tilde{b}\tilde{b}^*$ cross sections, the D0 results imply $m_{B'} \gtrsim 330$ GeV.

A later search for gluino pair production with $\tilde{g} \rightarrow b\bar{b}$ and $\tilde{b} \rightarrow b\tilde{\chi}_1^0$ has been carried out by the CDF Collaboration using 2.5 fb^{-1} collected luminosity. Candidate events were selected requiring two or more jets, large $\not{E}_T$, and at least two b-tags [32]. Using neural net analyses, CDF found $m_{\tilde{g}} > 350$ GeV (95% C.L.) for large mass splitting $\Delta m = m_{\tilde{g}} - m_{\tilde{b}} \gtrsim 80$ GeV, and about 340 GeV for small $\Delta m \sim 20$ GeV. Their result in the case of small mass splitting Δm can be applied to the $B'\bar{B}'$ search, implying roughly $m_{B'} \gtrsim 370$ GeV. Finally, there are also projections for squark searches at the LHC based on the $2j + \not{E}_T$ signal [33]. It is hard, however, to apply

their results to the $2b + \not{E}_T$ signal, since no b-tagging is used in that analysis.

In our analysis, we will focus on T' pair production, $pp(p\bar{p}) \rightarrow T'\bar{T}' \rightarrow t\bar{t}XX$, with the distinctive, but more complicated, final state of a top quark pair plus missing energy from the X particles. The CDF Collaboration has reported a search for the analogous supersymmetric process of top squark pair production based on an integrated luminosity of 2.7 fb^{-1}, using the purely leptonic final states from $p\bar{p} \rightarrow \tilde{t}_1\tilde{t}_1^*$, followed by $\tilde{t}_1 \rightarrow b\tilde{\chi}_1^\pm \rightarrow b\tilde{\chi}_1^0 l\nu$ [34]. The data are consistent with the SM, leading to the constraint $m_{\tilde{t}_1} \gtrsim 150$–185 GeV, where the exact limit depends on $m_{\tilde{\chi}_1^0}$, $m_{\tilde{\chi}_1^\pm}$, and $B(\tilde{\chi}_1^\pm \rightarrow \chi_1^0 l^\pm \nu)$. Similar signals also appear in other new physics scenarios such as little Higgs models with T-parity [16]. The $t\bar{t} + \not{E}_T$ signature at the LHC in the semileptonic channel has also been studied in Ref. [35]; however, that study focused on higher masses with larger integrated luminosity. The hadronic mode has been analyzed at the parton level in Ref. [36], focusing on the prospects for spin determination and mass measurements. In contrast, our study is performed at the detector level and is focused on the exclusion and discovery potential of both the Tevatron and early LHC data.

IV. EVENT SIMULATION, BACKGROUNDS, AND CUTS

A. Simulation

To investigate the discovery and exclusion prospects, we have simulated production and decay of the new particles at the Tevatron and at the LHC with $\sqrt{s} = 10$ TeV, as well as the main backgrounds. All simulations have been done using MADGRAPH/MADEVENT-PYTHIA 6.4.20-PGS4 [37–39] with the p_T-ordered PYTHIA showers and the CDF or ATLAS detector cards for PGS4. Matrix element/parton shower matching has been applied both for signal and backgrounds, and its validity has been double-checked by comparing different maximum multiplicity samples. The parton distribution function set used is CTEQ6L1, and factorization and renormalization scales are set to $\mu_F^2 = \mu_R^2 = m_T^2 = m^2 + p_T^2$ for the centrally produced particle pair. We do not apply K-factors for higher order QCD effects to either signal or background. These K-factors are expected to enhance these cross sections and be similar for the signal and top pair production (the dominant background after cuts), and hence the effect of including them would only be to increase the signal significance. In addition, there are uncertainties in the cross sections of both signal and backgrounds due to parton distribution functions [40].

For $m_{T'} - m_X < m_t$, the T' cannot decay to an on-shell $t + X$. These parameter points have therefore been simulated in MADGRAPH/MADEVENT using off-shell top decay, $T'\bar{T}' \rightarrow bW^+ X\bar{b}W^- X$. This procedure guarantees that finite width effects are correctly accounted for.

Note that QCD multijet backgrounds have not been simulated. Instead, we refer to the studies of Refs. [41,42] and apply similar cuts, in particular $\Delta\phi(\not{p}_T, p_T^j)$ cuts, $\not{E}_T$ cuts, and cuts on the number of jets, which should be enough to suppress the QCD multijet backgrounds to negligible levels.

The signatures of $pp(p\bar{p}) \rightarrow T'\bar{T}'$ are determined by the decays of the top quark pair and can therefore be divided into hadronic, semileptonic and purely leptonic channels. Since the T' decays will always generate missing transverse momentum from the invisible X particles in the final state, the most relevant backgrounds are those with significant missing energy from W or Z boson decays into neutrinos.

We will focus on the semileptonic and hadronic channels. The dilepton channel has suppressed cross section because of the small leptonic decay branching ratios. The semileptonic decay has the advantage that the presence of an isolated lepton (electron or muon) makes it easier to suppress QCD backgrounds, while for the fully hadronic channel this requires additional $\Delta\phi(\not{p}_T, p_T^j)$ cuts. This is particularly important for early running of the LHC, where the missing energy resolution might not yet be fully under control. On the other hand, the hadronic decay mode has larger branching ratio. Moreover, the main backgrounds, $t\bar{t}$ and $W^\pm$ production, only have substantial $\not{E}_T$ in association with leptons; in fact, the only truly irreducible background to the fully hadronic decay mode is $Z \rightarrow \nu\bar{\nu} +$ jets (and the negligible $t\bar{t}\nu\bar{\nu}$ background).

B. Semileptonic channel

To distinguish signal from background in the semileptonic case, we look for large $\not{E}_T$ and large transverse mass of the leptonic W candidate, defined to be

$$m_T^W \equiv m_T(p_T^l, \not{p}_T) = \sqrt{2|p_T^l||\not{p}_T|\cos(\Delta\phi(p_T^l, \not{p}_T))}.$$

Since the $\not{p}_T$ for the background is mainly from W decay, we expect $m_T^W < m_W$ for most of the background, while much of the signal extends beyond this limit. For the background surviving the $\not{E}_T$ and transverse mass cuts, we expect a significant fraction to be due to decays of the second top into hadronic τ leptons and missing energy. We therefore expect fewer jets for the background than for the signal. To further suppress the background, we also require the presence of a second, hadronically decaying W.

To implement this strategy, we employ the following precuts (differences between the Tevatron and the LHC are noted where they apply):

(i) One isolated electron or muon with $|p_T^l| > 10$ GeV.
(ii) No additional isolated leptons with $|p_T^l| > 2$ GeV.
(iii) Minimum missing transverse energy: $\not{E}_T > 100$ GeV.
(iv) Minimum transverse mass: $m_T^W > 100$ GeV.

(v) At least 4 jets with $|p_T^j| > 20$ GeV (Tevatron) or $|p_T^j| > 40$ GeV (LHC).
(vi) At least one jet pair with invariant mass within the W mass window $|m_{jj} - m_W| < 10$ GeV.

We also use additional cuts to achieve the best signal significance:

(i) Additional m_T^W cut: $m_T^W > 150$ GeV (Tevatron) or $m_T^W > 150, 200$ GeV (LHC).
(ii) Additional $\not{E}_T$ cuts: $\not{E}_T > 150$ GeV (Tevatron); $\not{E}_T > 150, 200, 250$ GeV (LHC).
(iii) $H_T = \sum_{i=1}^{4} |p_T^j|_i + |p_T^l|$ cuts: $H_T > 300$ GeV (Tevatron); $H_T > 400, 500$ GeV (LHC).
(iv) Combinations of the cuts above.

The relevant backgrounds for the semileptonic channel are $t\bar{t}$ (semileptonic and purely leptonic decays) and leptonically decaying $W^\pm +$ jets production. Top pairs are the main background. Because this has the same number of b-quarks as the signal, no b-tagging information is employed, since this would suppress signal and background by the same amount, leading to a reduced signal significance. For completeness, we also simulated $Z +$ jets (where the largest contribution comes from $Z \rightarrow \tau^+\tau^-$ with one of the taus decaying leptonically) and $t\bar{t}Z$, but these processes both turned out to be negligible after precuts.

We show the distributions for missing transverse energy $\not{E}_T$, transverse mass m_T^W, number of jets N(jets), and jet pair invariant mass m_{jj} for example signal parameters and backgrounds for the 10 TeV LHC in Fig. 1. Each observable is plotted after the cuts coming before it in the list, and the position of the precut is marked with a vertical dashed line. For clarity, we have split the $t\bar{t}$ background into components: semileptonic decays (to electron or muon), decays with at least one tau lepton, purely leptonic decays (where both W's decay to electron or muon) and fully hadronic decay (which is negligible with these cuts). The m_{jj} plot shows the invariant mass for the jet pair closest to the W mass. The corresponding distributions for the Tevatron are qualitatively similar.

The combined background cross section after precuts is 2.4 fb for the Tevatron, and 82 fb for the 10 TeV LHC. Typical signal efficiency for the precuts is 2–4% at the Tevatron and 1–2% at the LHC. The cross sections after cuts, for the main backgrounds and some example signal parameters, are found in the Appendix in Tables I and II. Significances and signal and background cross sections after near-optimal cuts for some signal points are found in Tables V and VI.

C. Hadronic channel

For the fully hadronic case, the background is mainly leptonic W decays (from $W +$ jets and $t\bar{t}$), where the lepton is either missed (or nonisolated) or a τ lepton has been mistagged as a jet, and $Z +$ jets, where the Z decays to neutrinos. We therefore expect the background to have
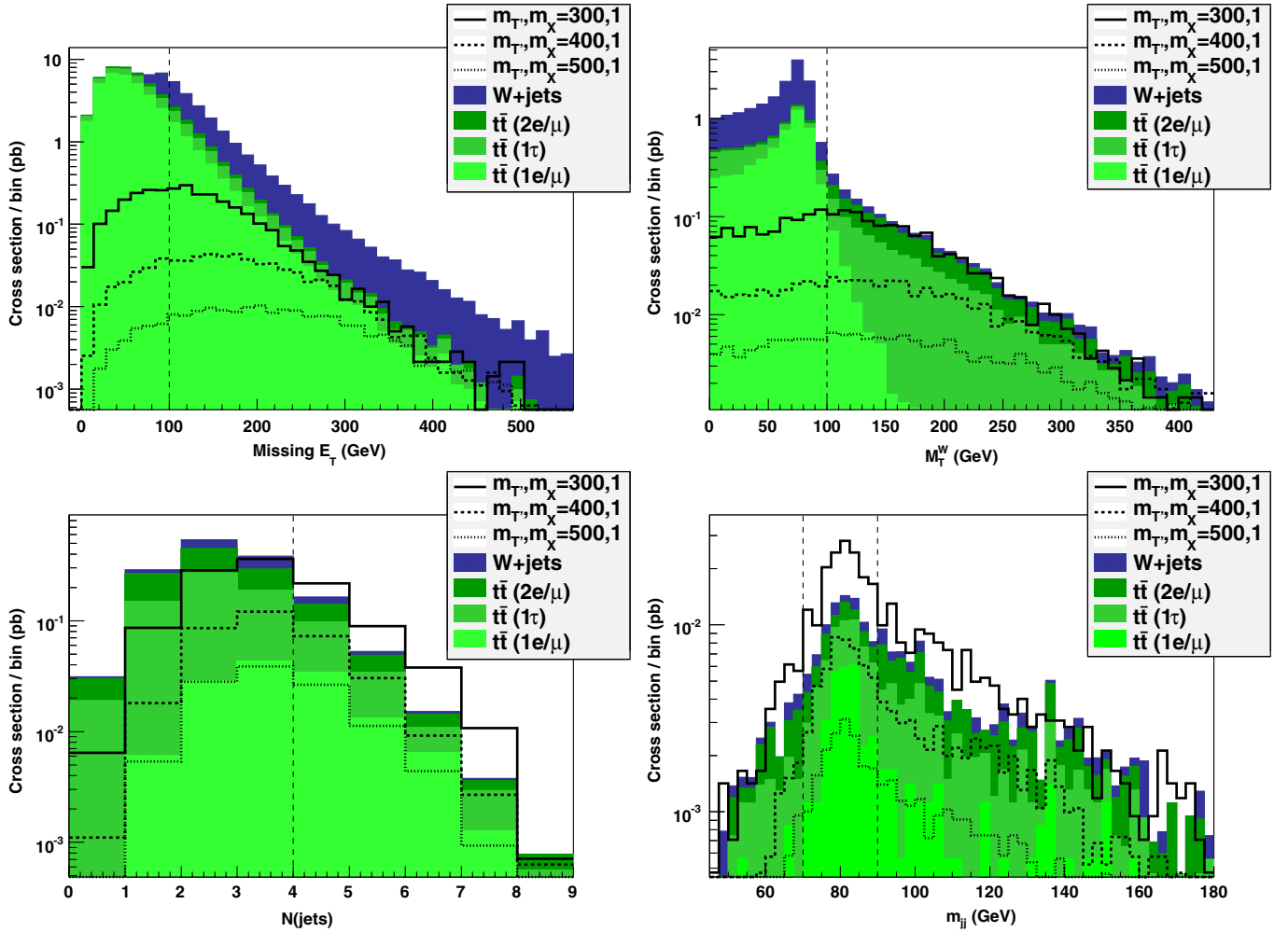
FIG. 1 (color online). Distributions of missing transverse energy $\not{E}_T$, transverse mass m_T^W, number of jets N(jets), and jet pair invariant mass m_{jj} for signal and backgrounds for the 10 TeV LHC in the semileptonic channel. Each of the observables has been plotted after the precuts coming before it in the list, and the chosen precut has been marked by a vertical line. For signal, the masses $(m_{T'}, m_X) = (300$ GeV, 1 GeV), (400 GeV, 1 GeV), and (500 GeV, 1 GeV) have been chosen for illustration. The W and Z samples were simulated with a cut on $\not{E}_T > 80$ GeV and at least 3 jets in the parton-level generation. See text for details.

fewer jets than the signal, which mainly consists of fully hadronic top decays, with missing energy from the invisible X particles. To be sure to avoid QCD multijet background, we also need to apply $\Delta\phi(\not{p}_T, p_T^j)$ cuts between the hardest jets and the missing energy. In fact, this also helps to reduce the $W \to \tau\nu$ background, since with large $\not{E}_T$ cuts, the W tends to be boosted, while the tau jet tends to be in the direction of the missing energy. The signal is furthermore expected to have larger $H_T = \sum |p_T^j|$ than the background.

For the fully hadronic channel, we use the following precuts:

(i) No isolated electrons, muons, or tau-tagged jets with $|p_T^l| > 2$ GeV.

(ii) Minimum missing transverse energy: $\not{E}_T > 100$ GeV.

(iii) At least 5 jets with $|p_T^j| > 20$ GeV (Tevatron) or $|p_T^j| > 40$ GeV (LHC).

(iv) Minimum $\Delta\phi(\not{p}_T, p_T^j)$ for the leading jets: $\Delta\phi(\not{p}_T, p_T^{j1}) > 90°$ and $\Delta\phi(\not{p}_T, p_T^{j2}) > 50°$ (Tevatron); $\Delta\phi(\not{p}_T, p_T^j) > 11.5°$ for the first, second, and third leading jets (LHC).

We also use the following additional cuts to optimize the signal significance:

(i) Additional $\not{E}_T$ cuts: $\not{E}_T > 150, 200, 250$ GeV (Tevatron); $\not{E}_T > 150, 200, 250, 300$ GeV (LHC).

(ii) $H_T = \sum_{i=1}^{5} |p_T^j|_i$ cuts: $H_T > 300, 350, 400$ GeV (Tevatron); $H_T > 400, 500$ GeV (LHC).

(iii) At least 6 jets with $|p_T^j| > 20$ GeV (Tevatron) or $|p_T^j| > 40$ GeV (LHC).

As discussed above, the relevant backgrounds for the fully hadronic channel are $t\bar{t}$, leptonically decaying $W^{\pm} +$ jets, and $Z \to \nu\bar{\nu} +$ jets. For completeness, we also simulated $t\bar{t}Z$, but this is negligible because of its small cross section. Among the $t\bar{t}$ decay modes, the dominant background is from decays with at least one tau lepton, fol-

lowed by the semileptonic decay to electron or muon (where the lepton is either missed or nonisolated).

Distributions for $\not{E}_T$, N(jets), and H_T for both signal and backgrounds in the hadronic channel at the 10 TeV LHC are shown in Fig. 2. The top two panels show $\not{E}_T$ and N(jets) plotted after the cuts coming before it in the list, and the position of the precut is marked with a vertical dashed line. The bottom two panels are $\not{E}_T$ and H_T distributions plotted after precuts. For clarity, we have split the $t\bar{t}$ background into components: fully hadronic decay (negligible after $\not{E}_T$ cut), decays with at least one tau lepton, semileptonic decays (to electron or muon), and purely leptonic decays (which are negligible with these cuts). The corresponding distributions for the Tevatron are qualitatively similar.

After precuts for the hadronic channel, the combined background cross section is 21 fb for the Tevatron and

1.4 pb for the 10 TeV LHC. The signal efficiency of the precuts is 9–20% at the Tevatron and 8–13% at the LHC. A table of cross sections after cuts for backgrounds and some signal points may be found in the Appendix in Tables III and IV. Significances and signal and background cross sections after near-optimal cuts for some signal points are found in Tables VII and VIII.

The main remaining backgrounds after precuts for both the semileptonic and hadronic channels include tau leptons. One reason for this is that a tau lepton is often mistagged as a jet, which therefore adds significantly to the fully hadronic background with large $\not{E}_T$ (in particular for the hadronic channel). It would be interesting to see an experimental study of whether an antitau tag could be effective in further suppressing these backgrounds, while keeping a good signal efficiency. This might be of signifi-
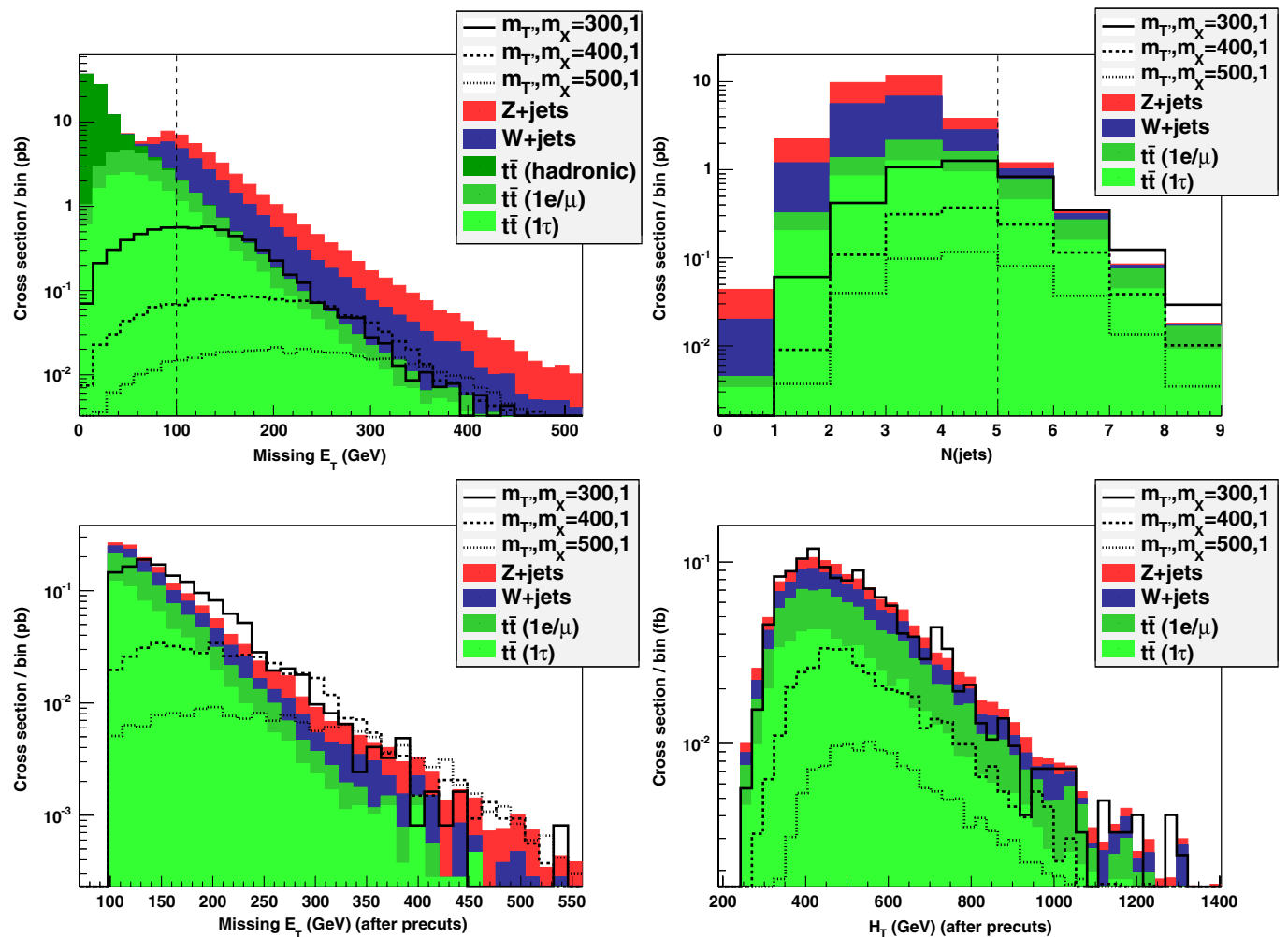

FIG. 2 (color online). $\not{E}_T$, N(jets), and H_T distributions for signal and backgrounds for the 10 TeV LHC in the hadronic channel. The top two panels show distributions of $\not{E}_T$ and N(jets) after the previous cuts in the precut table, with the position of the precut marked with a vertical dashed line. The lower two panels show distributions of $\not{E}_T$ and H_T after all precuts. The hadronic top contribution is negligible after the $\not{E}_T > 100$ GeV cut and has therefore been omitted in the remaining plots. For signal, the masses $(m_{T'}, m_X) =$ (300 GeV, 1 GeV), (400 GeV, 1 GeV), and (500 GeV, 1 GeV) have been chosen for illustration. The W and Z samples were simulated with a cut on $\not{E}_T > 80$ GeV and at least 3 jets in the parton-level generation. See text for details.
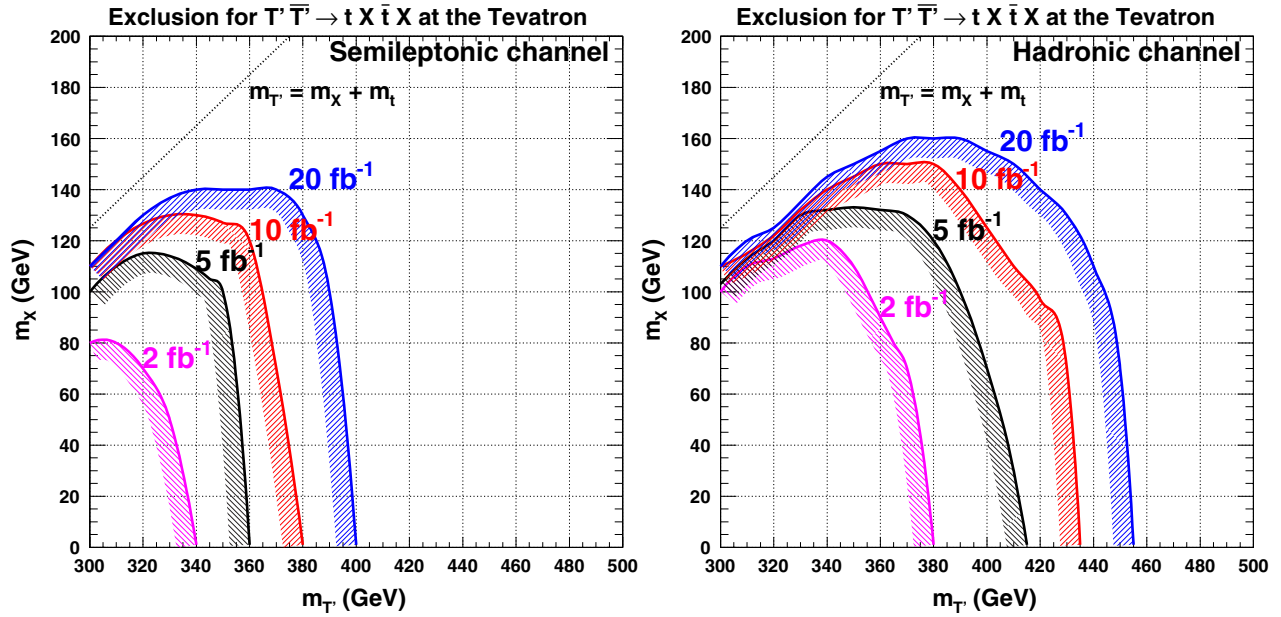
FIG. 3 (color online). 95% C.L. Tevatron exclusion contours for the semileptonic channel (left) and the hadronic channel (right) for integrated luminosities 2, 5, 10, and 20 fb^{-1}. For each point in parameter space, the cut with the best significance has been chosen.

cant importance for any new physics with signatures consisting of jets and missing energy.

V. DISCOVERY AND EXCLUSION REACH FROM TEVATRON AND EARLY LHC DATA

We now determine the discovery and exclusion reach for T' at the Tevatron and the 10 TeV LHC. For each parameter point $(m_{T'}, m_X)$, we use the optimum cut (after precuts) that gives the best signal significance, with the additional requirements that $S/B > 0.1$ and more than two signal events are observed. Given the small number of signal and background events after cuts, we have used Poisson statistics, rather than assuming Gaussian distributions, for both signal and backgrounds.

Figure 3 shows the 95% C.L. Tevatron exclusion contours for both the semileptonic and hadronic channels and integrated luminosities of 2, 5, 10, and 20 fb^{-1}. Even with just 2 fb^{-1}, exclusion limits of $m_{T'} > 340$ GeV (semileptonic mode) and $m_{T'} > 380$ GeV (hadronic mode) can be reached, which already extend into the interesting mass range consistent with current direct search bounds and precision electroweak data. With a combined integrated luminosity of 20 fb^{-1} at the end of Tevatron running, a reach of up to 455 GeV for the hadronic channel can be achieved.

The reach in $m_{T'}$ is almost independent of m_X for small to medium m_X. However, when m_X approaches the on-shell decay threshold of $m_{T'} - m_t$, the reach is limited since the top and X are produced nearly at rest in the T' rest frame, and the $T'\bar{T}'$ system therefore needs a transverse boost for the X particles to produce large missing transverse momentum. This leads to the dip in the exclusion

curves at m_X close to $m_{T'} - m_t$, and indeed there is no exclusion reach at the Tevatron for $m_{T'} - m_t - m_X \lesssim 15$ GeV. For 20 fb^{-1} integrated luminosity and $m_{T'}$ between 370 and 390 GeV, m_X could be excluded up to 160 GeV at 95% C.L. using the hadronic mode. For smaller $m_{T'}$, the reach in m_X is decreased due to the softness of the X particle distributions, while for larger $m_{T'}$, it is decreased because of the small $T'\bar{T}'$ production cross section.

Figure 4 shows the 3σ (Gaussian equivalent[2]) Tevatron discovery contours for both the semileptonic and hadronic channels for integrated luminosities of 2, 5, 10, and 20 fb^{-1}. A 3σ signal could be observed for $m_{T'} < 360$ GeV and $m_X \lesssim 110$ GeV in the semileptonic channel with 20 fb^{-1} integrated luminosity. The hadronic channel is more promising. With 5 fb^{-1} integrated luminosity, a reach in $m_{T'}$ up to 360 GeV could be achieved when m_X is not too large. With 20 fb^{-1} integrated luminosity, the reach is extended to 400 GeV for m_X up to about 80 GeV. For larger m_X, the reach in $m_{T'}$ decreases.

Figure 5 shows the 95% C.L. exclusion contours for a 10 TeV early LHC run, in the semileptonic and hadronic channels for integrated luminosities 100, 200, and 300 pb^{-1}. With just 100 pb^{-1}, the LHC exclusion reach for $m_{T'}$ exceeds the Tevatron exclusion reach with 20 fb^{-1} luminosity. Exclusions of $m_{T'}$ up to 490, 520, and 535 GeV could be achieved with 100, 200, and 300 pb^{-1} integrated luminosity for the semileptonic channel. The exclusion region for the hadronic channel covers almost the entire

---

[2]By Gaussian equivalent, we mean that we have converted the one-sided Poisson probability into the equivalent σ deviation in a two-sided Gaussian distribution, which is more commonly used in the literature.
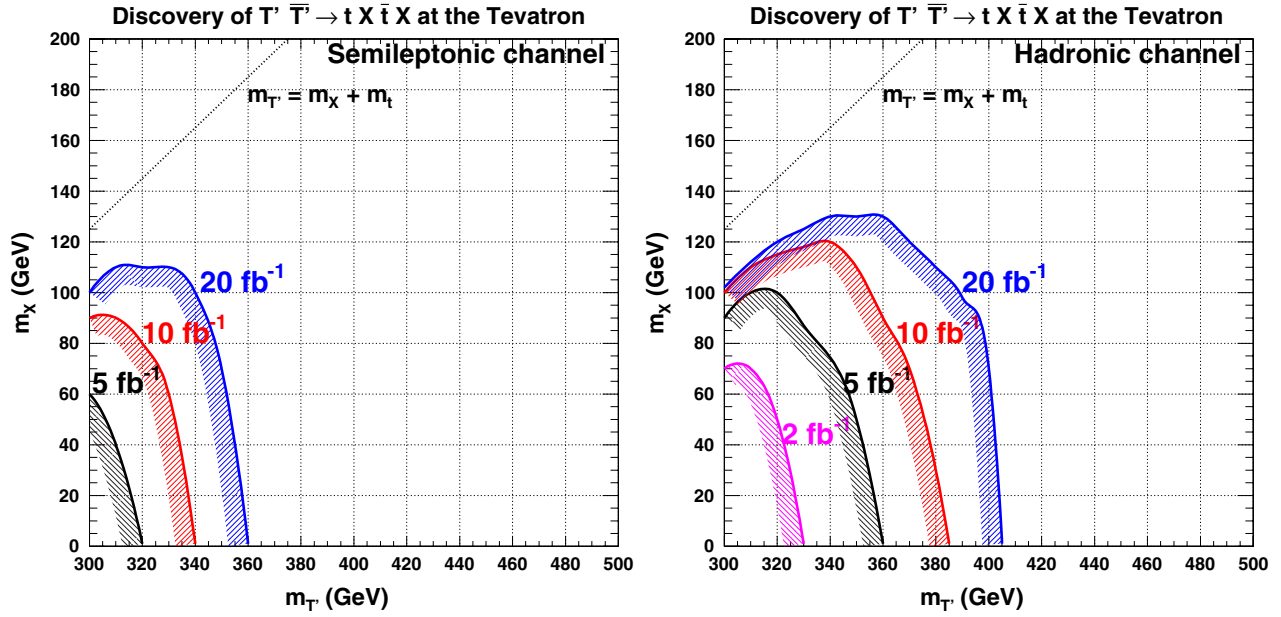
FIG. 4 (color online). 3σ (Gaussian equivalent) Tevatron discovery contours for the semileptonic channel (left) and the hadronic channel (right) for integrated luminosities 2, 5, 10, and 20 fb^{-1}. For each point in parameter space, the cut with the best significance has been chosen.

interesting mass parameter space with 300 pb^{-1} luminosity. Note that at the LHC, we could tolerate much smaller $m_{T'} - m_X$; in particular, we start probing the off-shell decay region $T' \to t^* X \to bWX$ for $m_{T'} - m_X < m_t$.

Figure 6 shows the 3σ (Gaussian equivalent) discovery contours for a 10 TeV LHC run, in the semileptonic and hadronic channels for integrated luminosities 100, 200, and 300 pb^{-1}. Although the reach in both $m_{T'}$ and m_X is limited for the semileptonic mode, the hadronic channel

could provide a 3σ signal for $m_{T'} \lesssim 490$ GeV and $m_X \lesssim 170$ GeV with 300 pb^{-1} luminosity. We might also observe a positive signal for m_X up to about 170 GeV in the off-shell decay region ($m_{T'} - m_X < m_t$) for $m_{T'} \lesssim 330$ GeV.

It is clear from the discovery and exclusion contours, both for the Tevatron and the LHC, that the fully hadronic channel has considerably larger reach than the semileptonic channel, for reasons enumerated in Sec. IV. In this channel, the full, currently viable, region in parameter
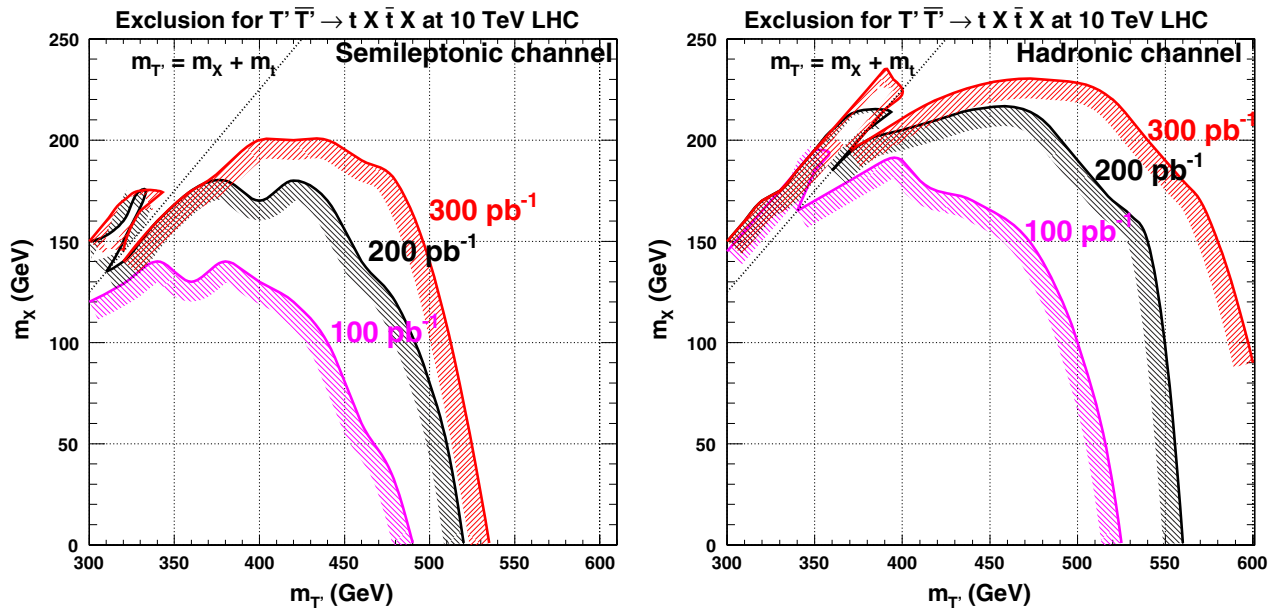

FIG. 5 (color online). 95% C.L. exclusion contours for a 10 TeV LHC run in the semileptonic channel (left) and the hadronic mode (right), for integrated luminosities 100, 200, and 300 pb^{-1}. For each point in parameter space, the cut with the best significance has been chosen.
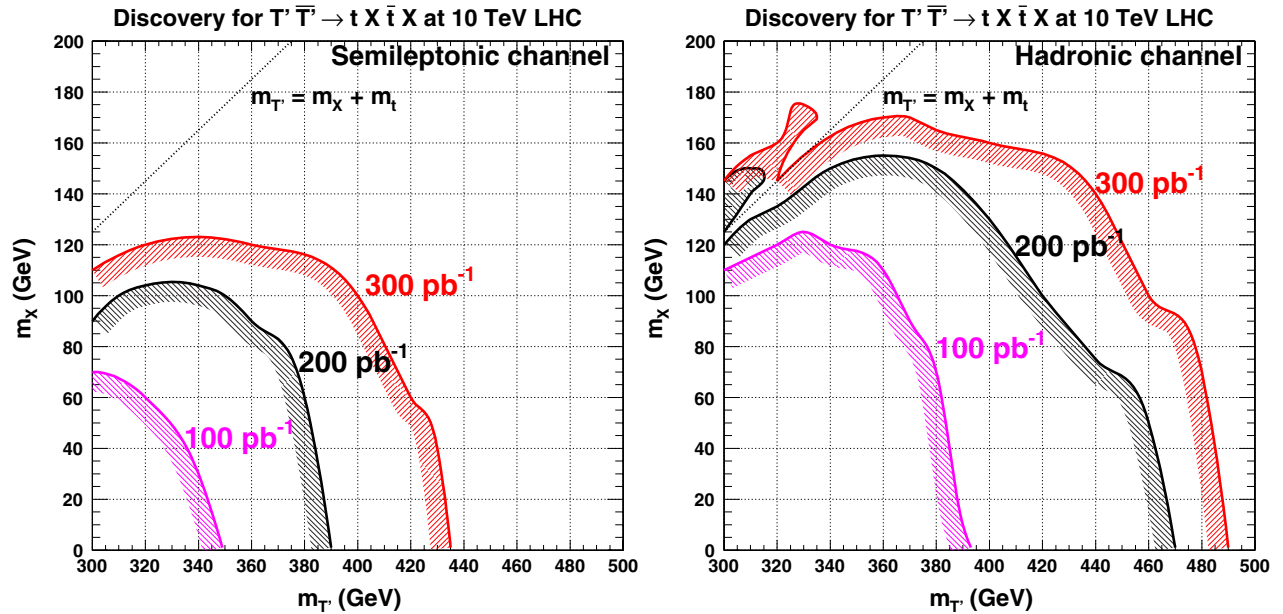
FIG. 6 (color online). 3σ (Gaussian equivalent) discovery contours for a 10 TeV LHC run, in the semileptonic channel (left) and the hadronic channel (right), for integrated luminosities 100, 200, and 300 pb^{-1}. For each point in parameter space, the cut with the best significance has been chosen.

space can be excluded at a 10 TeV LHC run.[3] In case both channels are visible, they can be used to distinguish between different model and mass hypotheses.

VI. CONCLUSIONS

We have considered the prospects for hadron colliders to pair produce new exotic quarks that decay directly to a pair of dark matter particles and SM particles. Although we have a particular interest in the WIMPless dark matter scenario [7] (including a specific example [8] that can potentially explain the DAMA annual modulation result), this scenario is motivated on quite general grounds, and, with minor modifications, our analysis applies to many other dark matter scenarios and other new physics models.

We have focused on the up-type exotic quark T'. T' pair production leads to $T'\bar{T}' \to t\bar{t}XX$, and we have then analyzed the semileptonic and fully hadronic channels. The fully hadronic channel (vetoing events with leptons) seems to be the most efficient, because of the large branching fraction and the reduction in SM background with large $\not{E}_T$.

Existing constraints require 300 GeV $\lesssim m_{T'} \lesssim$ 600 GeV, where the lower bound comes from direct searches, and the upper bound is from perturbativity. We have found that there are bright prospects for probing new

exotic quarks in this mass window at the Tevatron and in early data from the LHC. For models with $m_X \lesssim 120$ GeV, the discovery of new physics is possible at the Tevatron with ~ 10 fb^{-1} of luminosity, while for $m_X \lesssim 170$ GeV the discovery of new physics may be possible at the LHC with ~ 300 pb^{-1}. In particular, with ~ 300 pb^{-1} of data, the LHC should be able to discover almost all of the relevant parameter space with $m_X \lesssim 10$ GeV, where WIMPless models can explain the DAMA and CoGeNT results. Conversely, if no signal is seen in 300 pb^{-1}, the entire mass range consistent with current bounds and perturbativity will be excluded.

Of course, although an exclusion definitively excludes the model, a discovery will only be a discovery of a multi-jet (+lepton) + $\not{E}_T$ signal. Considerably larger integrated luminosity would be needed to identify the signal as $t\bar{t}$ + $\not{E}_T$, and it is an even harder problem to determine if the new physics really is $T'\bar{T}'$ production, with decay to top quarks and dark matter. Such a discovery analysis would require a good identification of the decaying top quarks as well as spin and mass determinations of the T' and X particles, and would require significant amounts of data from the LHC (and be beyond the capabilities of the Tevatron). New exotic quark decays are not the only processes that give a signal of top quark pairs plus missing transverse energy. In particular, this is a typical signature for supersymmetry, for example, from stop pair production followed by the decay $\tilde{t} \to t\tilde{\chi}_1^0$. However, it should be possible to distinguish these possibilities with more LHC data. Since the new exotic quark is a fermion, it has a higher production cross-section than squarks with a similar mass. Moreover, squarks could also have more complicated de-

---

[3] The results obtained here can be readily translated to an LHC run at 7 TeV, by multiplying the integrated luminosities needed by roughly a factor of 3. This approximation accounts for the difference in cross sections at different center of mass energies, assuming that the cut efficiencies for both the signal and backgrounds do not change significantly.

cay chains that would be absent in T' decay. There have already been studies on how to distinguish supersymmetric signals from other new physics with similar signals [35,36,43], and it would be worthwhile to perform a more detailed analysis of how one would distinguish new exotic quarks from squarks. It is also worth noting that the process $pp \rightarrow T'\bar{T}' \rightarrow X\bar{X}$ + jets would be well suited for analysis using the m_{T2} kinematic variable [44].

This analysis has focused on pair production of the up-type exotic quarks T'. Precision electroweak constraints imply that the down-type exotic quark B' must be fairly degenerate with the T', and so $B'\bar{B}' \rightarrow b\bar{b}X\bar{X}$ should also be accessible. This will likely be a more difficult signal to extract from early data, since it requires a good understanding of b-tagging, and we would expect large QCD backgrounds. But in the event of a discovery, such an analysis will be immensely useful in understanding the underlying physics.

There is also an interesting complementarity between the collider studies of dark matter considered here, and direct or indirect detection strategies. For example, one may consider WIMPless dark matter models in the limit of small λ. In this limit the cross sections for dark matter-nucleon scattering and for dark matter annihilation are small, and direct or indirect dark matter searches will be unsuccessful. But the production cross section for $T'\bar{T}'$ pairs is controlled by QCD, independent of the Yukawa coupling λ. So for models in this limit of parameter space, hadron colliders may provide the only direct evidence for the nature of dark matter. Interestingly, at small λ, the new exotic quarks are long-lived. This may result in displaced decay vertices, and a sufficiently long-lived new exotic quark may even hadronize and reach the detector. There has already been significant study of detection strategies for long-lived exotic hadrons [45], and these results should be directly applicable to the case when the T' travels a macroscopic distance in the detector. It would be interesting to investigate further how to determine the nature of such semistable color triplet particles.

Our results for a 10 TeV LHC run can be approximately translated to the alternative of an extended 7 TeV run. In this case, a coverage corresponding to the 300 pb^{-1} quoted in this study should be attainable for less than about 1 fb^{-1}.

Finally, and of particular interest, the annual modulation signal of DAMA [13] has been recently supported by unexplained events from CoGeNT [14], which, if interpreted as dark matter, also favor the same low mass $m_X \sim$ 5–10 GeV and high cross section $\sigma_{\rm SI} \sim 10^{-4}$ pb region of dark matter parameter space. These results are consistent with recent bounds and results from CDMS [15]. The consistency of several direct detection experiments is, of course, important to establish a dark matter signal. Improved statistics will be essential, but given the difficulty of making definitive background determinations, independent confirmation by completely different means is

also highly desirable. As discussed above, the direct detection data may naturally be explained by scalar dark matter interacting with new exotic quarks. Data already taken by the Super-Kamiokande experiment provide a promising probe of these interpretations of DAMA, CDMS, and CoGeNT through indirect detection [46]. The results derived here show that these explanations, including WIMPless models, can also be tested very directly with data already taken at the Tevatron and have extraordinarily promising implications for early runs of the LHC.

APPENDIX: IMPACT OF CUTS ON SIGNAL AND BACKGROUNDS

In this Appendix, we present tables listing the cross sections after cuts for the $T'\bar{T}'$ signal and the main SM backgrounds (Tables I, II, III, and IV). In the upper section of each table, each line gives the cross section after including all cuts above. In the lower section, each line gives the cross section after including the cut on that line, and all precuts. For the signal, three examples with $m_X = 1$ GeV

TABLE I. Signal and background cross sections in fb after cuts for the semileptonic channel at the Tevatron. The signal examples are for $m_X = 1$ GeV and $m_{T'} = 300$, 400, and 500 GeV as indicated. The W cross sections in parentheses were simulated with a cut on $\not{E}_T > 80$ GeV and at least 3 jets in the parton-level generation.

Cut	T' (300)	T' (400)	T' (500)	$t\bar{t}$	W + jets
No cut	203.2	16.33	1.11	5619	(5179)
1 μ/e, no τ	36.1	2.88	0.194	1041	(2060)
$\not{E}_T > 100$ GeV	17.7	2.00	0.157	107.2	(728.8)
$m_T^W > 100$ GeV	10.7	1.38	0.114	22.6	(36.62)
≥ 4 jets	4.81	0.64	0.062	2.6	0.30
$|m_{jj} - m_W| < 10$ GeV	4.13	0.51	0.049	2.2	0.19
All precuts	4.13	0.51	0.049	2.19	0.19
$m_T^W > 150$ GeV	1.93	0.325	0.036	0.62	0.035
$\not{E}_T > 150$ GeV	1.75	0.367	0.041	0.281	0.035
$H_T > 300$ GeV	1.93	0.353	0.042	1.18	0.07
$\not{E}_T > 150$, $H_T > 300$	1.04	0.279	0.037	0.056	0.017

TABLE II.   As in Table I, but for the semileptonic channel at the 10 TeV LHC and with cross sections in pb.

Cut	T' (300)	T' (400)	T' (500)	$t\bar{t}$ (1 e/μ)	$t\bar{t}$ (1 τ)	$t\bar{t}$ (2 e/μ)	W + jets
No cut	14.89	3.16	0.922	66.67	43.96	10.62	(42.28)
1 μ/e, no τ	3.2	0.669	0.193	36.45	8.15	3.18	(15.74)
$\not{E}_T > 100$ GeV	1.92	0.52	0.165	5.05	2.07	0.888	(10.33)
$m_T^W > 100$ GeV	1.1	0.342	0.116	0.134	0.638	0.471	(0.235)
≥ 4 jets	0.357	0.116	0.043	0.056	0.091	0.062	0.028
$|m_{jj} - m_W| < 10$ GeV	0.165	0.049	0.016	0.026	0.03	0.014	0.01
All precuts	0.165	0.049	0.016	0.027	0.031	0.014	0.01
$m_T^W > 150$ GeV	0.081	0.033	0.012	0.001	0.015	0.006	0.002
$m_T^W > 200$ GeV	0.032	0.019	0.008	0	0.006	0.003	0.001
$\not{E}_T > 150$ GeV	0.099	0.036	0.014	0.005	0.012	0.005	0.004
$\not{E}_T > 200$ GeV	0.040	0.025	0.010	0.001	0.004	0.001	0.002
$\not{E}_T > 250$ GeV	0.016	0.013	0.007	0	0.002	0.001	0.002
$H_T > 400$ GeV	0.107	0.035	0.013	0.018	0.022	0.008	0.007
$H_T > 500$ GeV	0.059	0.021	0.009	0.011	0.014	0.004	0.005
$\not{E}_T > 150, H_T > 400$	0.067	0.027	0.012	0.004	0.01	0.004	0.003
$\not{E}_T > 150, H_T > 500$	0.037	0.016	0.008	0.003	0.007	0.002	0.002
$\not{E}_T > 200, H_T > 400$	0.032	0.02	0.009	0.001	0.004	0.001	0.002
$\not{E}_T > 200, H_T > 500$	0.02	0.013	0.007	0	0.004	0.001	0.002
$\not{E}_T > 250, H_T > 400$	0.014	0.012	0.006	0	0.002	0.001	0.002
$\not{E}_T > 250, H_T > 500$	0.009	0.008	0.005	0	0.002	0.001	0.001

TABLE III.   As in Table I, but for the hadronic channel at the Tevatron and with cross sections in fb. The Z cross-sections in parentheses were simulated with a cut on $\not{E}_T > 80$ GeV and at least 3 jets in the parton-level generation.

Cut	T' (300)	T' (400)	T' (500)	$t\bar{t}$	W + jets	Z + jets
No cut	203.24	16.33	1.11	5619.1	(5179.06)	(3030.09)
0 isolated leptons	82.88	6.97	0.499	2265.54	(1756.96)	(2545.12)
$\not{E}_T > 100$ GeV	42.86	5.28	0.422	125.93	(663.5)	(1219.22)
≥ 5 jets	22.64	3.07	0.273	22.11	3.3	2.6
$\Delta\phi$ cuts	19.0	2.74	0.245	15.8	2.8	2.2
All precuts	19	2.74	0.245	15.8	2.8	2.2
$\not{E}_T > 150$ GeV	7.93	2.04	0.21	4.32	0.791	0.93
$\not{E}_T > 200$ GeV	1.06	1.25	0.158	1.02	0.183	0.313
$\not{E}_T > 250$ GeV	0.142	0.516	0.109	0.347	0.025	0.162
$H_T > 300$ GeV	9.9	2.04	0.224	5.16	0.55	0.495
$H_T > 350$ GeV	4.92	1.37	0.182	2.72	0.208	0.162
$H_T > 400$ GeV	2.46	0.787	0.135	1.22	0.083	0.081
$\not{E}_T > 150, H_T > 300$	5.2	1.64	0.197	2.19	0.217	0.404
$\not{E}_T > 200, H_T > 300$	0.996	1.11	0.153	0.821	0.067	0.212
$\not{E}_T > 250, H_T > 300$	0.142	0.495	0.108	0.347	0.025	0.142
$\not{E}_T > 200, H_T > 350$	0.711	0.794	0.131	0.511	0.033	0.081
$\not{E}_T > 250, H_T > 350$	0.142	0.399	0.098	0.255	0.017	0.071
$N(\text{jets}) \geq 6$	8.45	1.3	0.125	3.1	0.333	0.212
$N(\text{jets}) \geq 6, \not{E}_T > 150$ GeV	3.62	0.957	0.107	0.948	0.092	0.101
$N(\text{jets}) \geq 6, \not{E}_T > 200$ GeV	0.467	0.583	0.08	0.237	0.025	0.04
$N(\text{jets}) \geq 6, H_T > 300$ GeV	4.84	0.995	0.116	1.28	0.092	0.081
$N(\text{jets}) \geq 6, H_T > 350$ GeV	2.34	0.683	0.097	0.693	0.05	0.02
$N(\text{jets}) \geq 6, H_T > 400$ GeV	1.16	0.364	0.072	0.328	0.017	0.01
$N(j), \not{E}_T, H_T > 6, 150, 300$	2.64	0.786	0.102	0.58	0.033	0.061

and $m_{T'} = 300$, 400, and 500 GeV are chosen. The W and Z cross sections in parentheses were simulated with a cut on $\displaystyle{\not}E_T > 80$ GeV and at least 3 jets in the parton-level generation. We also present tables listing the signal significance and signal and background cross sections after cuts (using a choice of final cut close to the optimal cut for the points listed), expressed in Gaussian-equivalent stan-

dard deviations, for some example parameter points (Tables V, VI, VII, and VIII).

For the LHC, we have divided the $t\bar{t}$ background according to decays: hadronic, single tau lepton, semileptonic (electron or muon), double leptonic (electron or muon), and double tau lepton. Only the contributing decay modes have been included in the table.

TABLE IV. As in Table I, but for the hadronic channel at the 10 TeV LHC and with cross sections in pb.

Cut	T' (300)	T' (400)	T' (500)	$t\bar{t}$ (1 τ)	$t\bar{t}$ (1 e/μ)	$t\bar{t}$ (had)	W + jets	Z + jets
No cut	14.89	3.16	0.922	43.96	66.67	104.59	(42.28)	(18.86)
0 isolated leptons	6.75	1.5	0.45	16.88	13.11	72.29	(16.8)	(15.71)
$\not{E}_T > 100$ GeV	4.15	1.21	0.394	3.91	2.67	0.097	(11.25)	(11.48)
≥ 5 jets	1.34	0.406	0.135	0.664	0.47	0.031	0.305	0.212
$\Delta\phi$ cuts	1.19	0.374	0.125	0.56	0.41	0.01	0.265	0.187
All precuts	1.19	0.374	0.125	0.56	0.41	0.01	0.265	0.187
$\not{E}_T > 150$ GeV	0.727	0.341	0.136	0.205	0.128		0.131	0.119
$\not{E}_T > 200$ GeV	0.291	0.231	0.107	0.069	0.042		0.06	0.069
$\not{E}_T > 250$ GeV	0.107	0.131	0.079	0.026	0.015		0.026	0.04
$\not{E}_T > 300$ GeV	0.043	0.062	0.053	0.011	0.005		0.014	0.022
$H_T > 400$ GeV	1.02	0.379	0.149	0.422	0.307		0.207	0.145
$H_T > 500$ GeV	0.668	0.264	0.118	0.275	0.209		0.133	0.096
$\not{E}_T > 150, H_T > 400$	0.6	0.301	0.128	0.176	0.109		0.113	0.1
$\not{E}_T > 150, H_T > 500$	0.411	0.213	0.103	0.129	0.082		0.078	0.071
$\not{E}_T > 200, H_T > 400$	0.271	0.21	0.103	0.065	0.039		0.056	0.062
$\not{E}_T > 200, H_T > 500$	0.213	0.152	0.085	0.053	0.03		0.042	0.049
$\not{E}_T > 250, H_T > 400$	0.106	0.126	0.078	0.026	0.015		0.025	0.038
$\not{E}_T > 250, H_T > 500$	0.097	0.096	0.067	0.024	0.012		0.021	0.031
$\not{E}_T > 300, H_T > 400$	0.043	0.06	0.053	0.011	0.005		0.014	0.021
$\not{E}_T > 300, H_T > 500$	0.043	0.05	0.048	0.011	0.005		0.013	0.019
$N(\text{jets}) \geq 6$	0.509	0.181	0.064	0.178	0.13		0.046	0.028
$N(\text{jets}) \geq 6, \not{E}_T > 150$	0.278	0.138	0.055	0.068	0.044		0.027	0.019
$N(\text{jets}) \geq 6, \not{E}_T > 200$	0.134	0.096	0.044	0.025	0.015		0.015	0.012
$N(\text{jets}) \geq 6, \not{E}_T > 250$	0.052	0.055	0.034	0.01	0.005		0.006	0.008
$N(\text{jets}) \geq 6, \not{E}_T > 300$	0.023	0.027	0.024	0.004	0.001		0.003	0.005
$N(\text{jets}) \geq 6, H_T > 400$	0.424	0.166	0.062	0.152	0.109		0.041	0.025
$N(\text{jets}) \geq 6, H_T > 500$	0.319	0.126	0.052	0.109	0.08		0.03	0.019
$N(j), \not{E}_T, H_T > 6, 150, 400$	0.25	0.128	0.053	0.063	0.04		0.025	0.018
$N(j), \not{E}_T, H_T > 6, 150, 500$	0.202	0.099	0.045	0.049	0.03		0.019	0.014
$N(j), \not{E}_T, H_T > 6, 200, 400$	0.126	0.09	0.043	0.024	0.014		0.014	0.012
$N(j), \not{E}_T, H_T > 6, 200, 500$	0.115	0.069	0.038	0.021	0.011		0.011	0.01
$N(j), \not{E}_T, H_T > 6, 250, 400$	0.051	0.054	0.033	0.01	0.005		0.006	0.007
$N(j), \not{E}_T, H_T > 6, 250, 500$	0.048	0.044	0.03	0.009	0.004		0.005	0.007
$N(j), \not{E}_T, H_T > 6, 300, 400$	0.023	0.027	0.023	0.004	0.001		0.003	0.005
$N(j), \not{E}_T, H_T > 6, 300, 500$	0.023	0.023	0.022	0.004	0.001		0.003	0.005

TABLE V. Significance after cuts for some example $(m_{T'}, m_X)$ points, for the semileptonic channel at the Tevatron, expressed in Gaussian-equivalent standard deviations. Cut used: precuts + $m_T^W > 150$ GeV.

	Before cuts		After cuts			
Benchmark points $(m_{T'}, m_X)$ (GeV)	σ_{sig} (fb)	σ_{bg} (fb)	σ_{sig} (fb)	σ_{bg} (fb)	S/B	Discovery significance $\mathcal{L} = 10$ fb^{-1}
(300,1)	203.2	>11 000	1.93	0.66	2.79	5.39σ
(400,1)	16.3		0.32		0.48	0.77σ
(400 100)	16.3		0.31		0.47	0.77σ

TABLE VI.   As in Table V, but for the semileptonic channel at the LHC, using cut: precuts + $\not{E}_T > 200$ GeV.

Benchmark points $(m_{T'}, m_X)$ (GeV)	Before cuts		After cuts			
	σ_{sig} (fb)	σ_{bg} (fb)	σ_{sig} (fb)	σ_{bg} (fb)	S/B	Discovery significance $\mathcal{L} = 0.2$ fb^{-1}
(300,1)	14900	>270 000	40.4	8.98	4.56	3.70σ
(400,1)	3160		25.4		2.81	2.32σ
(500,1)	922		10.3		1.15	0.62σ
(400 100)	3160		28.0		3.11	2.80σ
(400 200)	3160		11.3		1.25	1.24σ

TABLE VII.   As in Table V, but for the hadronic channel at the Tevatron, using cut: precuts + $\not{E}_T > 150$ GeV.

Benchmark points $(m_{T'}, m_X)$ (GeV)	Before cuts		After cuts			
	σ_{sig} (fb)	σ_{bg} (fb)	σ_{sig} (fb)	σ_{bg} (fb)	S/B	Discovery significance $\mathcal{L} = 10$ fb^{-1}
(300,1)	203.2	>13 800	7.93	5.96	1.37	7.99σ
(400,1)	16.3		2.04		0.36	2.47σ
(400 100)	16.3		1.72		0.29	1.99σ

TABLE VIII.   As in Table V, but for the hadronic channel at the LHC, using cut: precuts + $\not{E}_T > 150$ GeV.

Benchmark points $(m_{T'}, m_X)$ (GeV)	Before cuts		After cuts			
	σ_{sig} (fb)	σ_{bg} (fb)	σ_{sig} (fb)	σ_{bg} (fb)	S/B	Discovery significance $\mathcal{L} = 0.2$ fb^{-1}
(300,1)	14890	>290 000	727	584	1.24	$>10\sigma$
(400,1)	3160		341		0.58	5.79σ
(500,1)	922		136		0.23	2.40σ
(400 100)	3160		264		0.45	4.50σ
(400 200)	3160		95.0		0.16	1.61σ

[1] L. Ackerman, M. R. Buckley, S. M. Carroll, and M. Kamionkowski, Phys. Rev. D **79**, 023519 (2009).

[2] J. L. Feng, M. Kaplinghat, H. Tu, and H. B. Yu, J. Cosmol. Astropart. Phys. 07 (2009) 004.

[3] H. Goldberg, Phys. Rev. Lett. **50**, 1419 (1983); **103**, 099905(E) (2009).

[4] J. R. Ellis, J. S. Hagelin, D. V. Nanopoulos, K. A. Olive, and M. Srednicki, Nucl. Phys. **B238**, 453 (1984).

[5] G. Servant and T. M. P. Tait, Nucl. Phys. **B650**, 391 (2003).

[6] H. C. Cheng, J. L. Feng, and K. T. Matchev, Phys. Rev. Lett. **89**, 211301 (2002).

[7] J. L. Feng and J. Kumar, Phys. Rev. Lett. **101**, 231301 (2008).

[8] J. L. Feng, J. Kumar, and L. E. Strigari, Phys. Lett. B **670**, 37 (2008).

[9] R. Bernabei *et al.* (DAMA Collaboration), Eur. Phys. J. C **56**, 333 (2008).

[10] R. Bernabei *et al.*, Eur. Phys. J. C **67**, 39 (2010).

[11] See, e.g., M. Brhlik and L. Roszkowski, Phys. Lett. B **464**, 303 (1999); P. Belli, R. Bernabei, A. Bottino, F. Donato, N. Fornengo, D. Prosperi, and S. Scopel, Phys. Rev. D **61**, 023512 (1999); P. Gondolo and G. Gelmini, Phys. Rev. D **71**, 123520 (2005).

[12] R. Bernabei *et al.*, Eur. Phys. J. C **53**, 205 (2008); S. Chang, A. Pierce, and N. Weiner, Phys. Rev. D **79**, 115011 (2009); M. Fairbairn and T. Schwetz, J. Cosmol. Astropart. Phys. 01 (2009) 037.

[13] F. Petriello and K. M. Zurek, J. High Energy Phys. 09 (2008) 047; C. Savage, G. Gelmini, P. Gondolo, and K. Freese, J. Cosmol. Astropart. Phys. 04 (2009) 010.

[14] C. E. Aalseth *et al.* (CoGeNT Collaboration), arXiv:1002.4703.

[15] Z. Ahmed *et al.* (The CDMS-II Collaboration), arXiv:0912.3592.

[16] H. C. Cheng and I. Low, J. High Energy Phys. 08 (2004) 061.

[17] P. Fileviez Perez and M. B. Wise, arXiv:1002.1754.

[18] Ya. B. Zeldovich, Adv. Astron. Astrophys. **3**, 241 (1965); H. Y. Chiu, Phys. Rev. Lett. **17**, 712 (1966); G. Steigman, Annu. Rev. Nucl. Part. Sci. **29**, 313 (1979); R. J. Scherrer and M. S. Turner, Phys. Rev. D **33**, 1585 (1986); **34**, 3263(E) (1986).

[19] R. Foot, Phys. Rev. D **78**, 043529 (2008); M. Y. Khlopov and C. Kouvaris, Phys. Rev. D **78**, 065040 (2008); S. Andreas, T. Hambye, and M. H. G. Tytgat, J. Cosmol. Astropart. Phys. 10 (2008) 034; E. Dudas, S. Lavignac, and J. Parmentier, Nucl. Phys. **B808**, 237 (2009); S.

Andreas, arXiv:0905.0785.

[20] T. Han and R. Hempfling, Phys. Lett. B **415**, 161 (1997).

[21] L. J. Hall, T. Moroi, and H. Murayama, Phys. Lett. B **424**, 305 (1998).

[22] D. Tucker-Smith and N. Weiner, Phys. Rev. D **64**, 043502 (2001); **72**, 063509 (2005).

[23] S. Nussinov, L. T. Wang, and I. Yavin, J. Cosmol. Astropart. Phys. 08 (2009) 037.

[24] A. Menon, R. Morris, A. Pierce, and N. Weiner, arXiv:0905.1847.

[25] See, e.g., V. A. Kudryavtsev, M. Robinson, and N. J. C. Spooner, J. Phys. Conf. Ser. **203**, 012039 (2010).

[26] A. Bottino, F. Donato, N. Fornengo, and S. Scopel, Phys. Rev. D **68**, 043506 (2003); **77**, 015002 (2008); **78**, 083520 (2008).

[27] M. A. Shifman, A. I. Vainshtein, and V. I. Zakharov, Phys. Lett. **78B**, 443 (1978).

[28] V. Barger, J. Kumar, D. Marfatia, and E. M. Sessolo, arXiv:1004.4573 [Phys. Rev. D (to be published)].

[29] H. J. He, N. Polonsky, and S. f. Su, Phys. Rev. D **64**, 053004 (2001); J. Alwall et al., Eur. Phys. J. C **49**, 791 (2007); G. D. Kribs, T. Plehn, M. Spannowsky, and T. M. P. Tait, Phys. Rev. D **76**, 075016 (2007); R. Fok and G. D. Kribs, Phys. Rev. D **78**, 075023 (2008); B. Holdom, W. S. Hou, T. Hurth, M. L. Mangano, S. Sultansoy, and G. Unel, PMC Phys. A **3**, 4 (2009); M. Hashimoto, Phys. Rev. D **81**, 075023 (2010).

[30] V. M. Abazov et al. (D0 Collaboration), Phys. Rev. Lett. **97**, 171806 (2006).

[31] T. Aaltonen et al. (CDF Collaboration), Phys. Rev. D **76**, 072010 (2007).

[32] T. Aaltonen et al. (CDF Collaboration), Phys. Rev. Lett. **102**, 221801 (2009).

[33] See, e.g., CMS Collaboration, Physics Analysis Summary SUS-08-005, http://cms-physics.web.cern.ch/cms-physics/public/SUS-08-005-pas.pdf.

[34] A. G. Ivanov (CDF Collaboration), arXiv:0811.0788.

[35] T. Han, R. Mahbubani, D. G. E. Walker, and L. T. E. Wang, J. High Energy Phys. 05 (2009) 117.

[36] P. Meade and M. Reece, Phys. Rev. D **74**, 015010 (2006).

[37] J. Alwall et al., J. High Energy Phys. 09 (2007) 028.

[38] T. Sjostrand, S. Mrenna, and P. Skands, J. High Energy Phys. 05 (2006) 026.

[39] John Conway, Pretty Good Simulation of High Energy Collisions, http://www.physics.ucdavis.edu/~conway/research/software/pgs/pgs4-general.htm.

[40] A. D. Martin, R. G. Roberts, W. J. Stirling, and R. S. Thorne, Eur. Phys. J. C **28**, 455 (2003); **35**, 325 (2004); P. M. Nadolsky et al., Phys. Rev. D **78**, 013004 (2008).

[41] V. M. Abazov et al. (D0 Collaboration), Phys. Lett. B **638**, 119 (2006).

[42] ATLAS Collaboration, report ATLAS Note ATL-PHYS-PUB-2009-084 (unpublished).

[43] A. Datta, K. Kong, and K. T. Matchev, Phys. Rev. D **72**, 096006 (2005); **72**, 119901 (2005).

[44] C. G. Lester and D. J. Summers, Phys. Lett. B **463**, 99 (1999); C. Lester and A. Barr, J. High Energy Phys. 12 (2007) 102; W. S. Cho, K. Choi, Y. G. Kim, and C. B. Park, Phys. Rev. Lett. **100**, 171801 (2008); A. J. Barr, B. Gripaios, and C. G. Lester, J. High Energy Phys. 02 (2008) 014; M. M. Nojiri, Y. Shimizu, S. Okada, and K. Kawagoe, J. High Energy Phys. 06 (2008) 035; M. Burns, K. Kong, K. T. Matchev, and M. Park, J. High Energy Phys. 03 (2009) 143; A. J. Barr and C. Gwenlan, Phys. Rev. D **80**, 074007 (2009).

[45] M. Drees and X. Tata, Phys. Lett. B **252**, 695 (1990); G. Aad et al. (ATLAS Collaboration), arXiv:0901.0512; P. Mermod (ATLAS Collaboration), AIP Conf. Proc. **1200**, 750 (2010).

[46] D. Hooper, F. Petriello, K. M. Zurek, and M. Kamionkowski, Phys. Rev. D **79**, 015010 (2009); J. L. Feng, J. Kumar, J. Learned, and L. E. Strigari, J. Cosmol. Astropart. Phys. 01 (2009) 032; J. Kumar, J. G. Learned, and S. Smith, Phys. Rev. D **80**, 113002 (2009); V. Niro, A. Bottino, N. Fornengo, and S. Scopel, Phys. Rev. D **80**, 095019 (2009).